Bio-Design and Manufacturing (2023) 6:373–389
https://doi.org/10.1007/s42242-022-00229-9

RESEARCH ARTICLE

3D-bioprinted cholangiocarcinoma-on-a-chip model for evaluating drug responses

Qiong Liu[1,2,3] · Luis S. Mille[1,4] · Cesar Villalobos[1,5] · Ingrid Anaya[1,5] · Matthias Vostatek[1,6] · Sili Yi[1] · Wanlu Li[1] · Junlong Liao[1] · Huanghui Wu[2,3] · Yongteng Song[2,7] · Lize Xiong[2,3] · Yu Shrike Zhang[1]

Received: 10 January 2022 / Accepted: 23 December 2022 / Published online: 22 March 2023

Abstract

Cholangiocarcinoma (CCA) is characterized by heterogeneous mutations and a refractory nature. Thus, the development of a model for effective drug screening is urgently needed. As the established therapeutic testing models for CCA are often ineffective, we fabricated an enabling three-dimensional (3D)-bioprinted CCA-on-a-chip model that to a good extent resembled the multicellular microenvironment and the anatomical microstructure of the hepato-vascular–biliary system to perform high-content antitumor drug screening. Specifically, cholangiocytes, hepatocytes, and vascular endotheliocytes were employed for 3D bioprinting of the models, allowing for a high degree of spatial and tube-like microstructural control. Interestingly, it was possible to observe CCA cells attached to the surfaces of the gelatin methacryloyl (GelMA) hydrogel-embedded microchannels and overgrown in a thickening manner, generating bile duct stenosis, which was expected to be analogous to the in vivo configuration. Over 4000 differentially expressed genes were detected in the CCA cells in our 3D coculture model compared to the traditional two-dimensional (2D) monoculture. Further screening revealed that the CCA cells grown in the 3D traditional model were more sensitive to the antitumoral prodrug than those in the 2D monoculture due to drug biotransformation by the neighboring functional hepatocytes. This study provides proof-of-concept validation of our bioprinted CCA-on-a-chip as a promising drug screening model for CCA treatment and paves the way for potential personalized medicine strategies for CCA patients in the future.

✉ Yu Shrike Zhang
yszhang@research.bwh.harvard.edu

1 Division of Engineering in Medicine, Department of Medicine, Brigham and Women's Hospital, Harvard Medical School, Cambridge, MA 02139, USA

2 Translational Research Institute of Brain and Brain-Like Intelligence, Shanghai Fourth People's Hospital, School of Medicine, Tongji University, Shanghai 200434, China

3 Shanghai Key Laboratory of Anesthesiology and Brain Functional Modulation, Shanghai 200434, China

4 Department of Bioengineering, Stanford University, Palo Alto, CA 94305, USA

5 Biotechnological Engineering Program, Monterrey Institute of Technology and Higher Education, 64849 Monterrey, Nuevo León, Mexico

6 Molecular Biotechnology, University of Applied Sciences Campus Vienna, 1100 Vienna, Austria

7 Rapid Manufacturing Engineering Center, School of Mechatronical Engineering and Automation, Shanghai University, Shanghai 200444, China

Graphic abstract

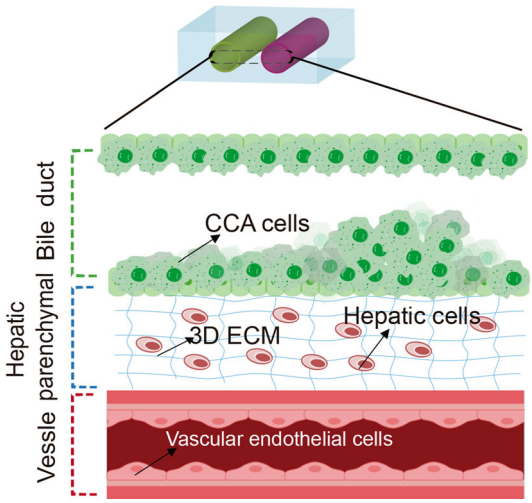

Keywords Tumor-on-a-chip · Biliary tumor · 3D bioprinting · Tumor microenvironment · Drug screening

Introduction

Cholangiocarcinoma (CCA) is an aggressive type of cancer with a poor prognosis due to its high heterogeneity and lack of effective therapeutic options. Traditionally, it is classified according to its anatomical locations as intrahepatic (iCCA), perihilar (pCCA), or distal (dCCA) [1]. Regardless of their location, sequencing analyses in CCA have revealed that this is a heterogeneous condition with a myriad of genetic mutations, some of which could be actionable, leading to the development of targeted precision therapy [2]. However, following this idea, only 0.4% of patients have been identified as potential candidates for United States Food and Drug Administration (FDA)-approved drugs, suggesting that current genetic methods are still insufficient to identify clinical treatments for most CCAs [3]. Therefore, the need for a higher-throughput and more efficient drug screening model that can bring reliable precision medicine diagnostics to CCA patients is urgent.

The tumor microenvironment (TME) plays a crucial role in the progression and invasiveness of CCA [4]. Unfortunately, partly due to the inability to recapitulate the in vivo microenvironment of a tumor, traditional two-dimensional (2D) monoculture approaches to cancer research have left dramatic gaps in our understanding of the tumor and our ability to develop effective antitumoral treatments. These gaps have caused the rising costs for anticancer drugs and the failure in 95% of clinical trials due to toxicity and/or inefficiency [5]. As a consequence, mouse models have become popular in reconstructing the TME and are an effective method of diagnosis and drug discovery. On the other hand, patient-derived xenograft (PDX) models are also commonly used, as they eliminate species-incompatibility [6]. However, they hardly control the anatomical microstructures, a problem that patient-derived orthotopic xenografts (PDOXs) can overcome, to some degree, by engrafting tumor specimens in the orthotopic sites of origin. Nevertheless, the high cost of time and low success rate are significant obstacles toward applying PDOXs for preclinical trials and personalized medicine [6].

Rapid ex vivo reconstruction of the complex CCA microenvironment would significantly advance CCA biology and tumor therapy. Three-dimensional (3D) tumor-on-a-chip platforms are promising candidates for replicating the TME, including the CCA microenvironment, since they can rapidly replicate both the structures and functions based on personalizable designs [7–10], unlike 2D and other conventional models. It has already been established that these high-content in vitro models can simulate complex mechanisms, such as the transport of pharmaceutical compounds, and therefore are thought to provide enhanced accuracy for anticancer drug screening [7]. Of note, tumor-on-a-chip models can incorporate a plethora of biological and chemical factors, including oxygen and pH levels and extracellular matrix (ECM) properties [11, 12]. In addition, these models can further form multiorgan-on-a-chip systems, which play a crucial role in mimicking in vivo tumor metastasis and systemic development [13–15].

Tumor-on-a-chip platforms can be further combined with bioprinting to harness both dynamic microenvironments and volumetric architectures [16]. Gelatin methacryloyl

(GelMA) is a versatile natural polymer-derived biomaterial that is amenable to both bioprinting and creating 3D TME-mimicry through on-chip configurations due to its ease of rapid, precisely controllable photopolymerization [17].

In this study, we demonstrated the utilization of 3D bioprinting technology to fabricate and assemble a microchannel-embedded CCA-on-a-chip model. This high-content traditional model simulated the microenvironment and microstructure of the orthotopic site more precisely than previous cell culture models and represented a more accurate depiction of the tissue-level effects of cyclophosphamide than a 2D tumor cell monoculture system.

Materials and methods

GelMA synthesis

GelMA was synthesized according to our previously published procedures [17, 18]. Briefly, porcine or fish gelatin type A (Sigma–Aldrich) was added to 100 mL of phosphate-buffered saline (PBS, Thermo Fisher) at 10% (mass fraction) and stirred at 50 °C until dissolved. For a methacryloyl-modification degree of 55%–65% (medium-GelMA, M-GelMA), 5 mL of methacrylic anhydride (MAA, Sigma–Aldrich, USA) was added. For a methacryloyl-modification degree of 90%–100% (high-GelMA, H-GelMA), this amount was increased to 8 mL. This solution was stirred at 50 °C for 1.5 h, after which the solution was diluted 2× with preheated PBS and left stirred for another 20 min. This solution was then dialyzed using Spectra/Por membrane tubing (molecular weight cut off: 12,000–14,000 kDa, Fisher Scientific) in deionized water at 40 °C for 7 days. The dialyzed GelMA was then filtered and lyophilized for 5 days. Freeze-dried GelMA foam was covered with aluminum foil and left overnight at −80 °C. It was then stored at 4 °C until used.

Cultivation of cells and construction of the transgenic cells

RBE cholangiocarcinoma cells (Elabscience Biotechnology) were cultured in Roswell Park Memorial Institute (RPMI) 1640 medium (Invitrogen), human umbilical vein endothelial cells (HUVECs, Angio-Proteomie) were cultured in endothelial cell medium (Lonza), and HepG2 cells (ATCC) were maintained in Dulbecco's modified Eagle medium (DMEM, Invitrogen). All cells were supplemented with 10% (volume fraction) fetal bovine serum (FBS, Invitrogen) and 1% (volume fraction) penicillin and streptomycin (pen/strep, Invitrogen) and cultured under standard conditions (37 °C in a humidified atmosphere, 5% CO_2). For the 3D chip model and 2D control model, the coculture medium was formulated at a 1:1:1 volume ratio of RBE/HUVEC/HepG2 culture media with vascular endothelial growth factor (VEGF) added at 10 ng/mL.

To visualize the living cells, pCMV-LifeAct-RFP or EGFP (Ibidi) was used to obtain red or green fluorescent protein (RFP or EGFP)-tagged LifeAct with a nontoxic actin-binding amino acid. Then, the LifeAct-RFP/EGFP-overexpressing lentivirus vector pH 5674-LifeAct-RFP/EGFP was constructed, as shown in Fig. S1a (Supplementary Information). The transgenic cell lines HUVEC-LifeAct-RFP and RBE-LifeAct-EGFP were finally obtained by lenti-LifeAct-RFP/EGFP transduction of HUVECs for the visualization of actin using a fluorescence microscope (Nikon) (Fig. S1b in Supplementary Information).

Fabrication of sacrificial bioprinting-based CCA-on-a-chip

For sacrificial bioprinting, agarose (Sigma–Aldrich) was used as the fugitive template to fabricate the microchannels in the GelMA constructs. Agarose microfibers were produced according to our previously published procedures [19]. Briefly, an agarose solution (10% (mass fraction) in PBS) heated at 80 °C was loaded into a glass capillary (0.3–1.6 mm in diameter) and then placed at room temperature to achieve gelation. GelMA solution (0.05, 0.075, or 0.09 g/mL) M- or H-GelMA in PBS) with lithium phenyl(2,4,6-trimethylbenzoyl)phosphinate (LAP, Allevi, 0.002 g/mL) was left to dissolve at 37 °C and then filtered using 0.2-μm syringe filters (Fisher Scientific). GelMA solution (mixed with HepG2 cells or not) was then poured into a predefined poly(methyl methacrylate) mold containing the bioprinted agarose filaments and placed under ultraviolet (UV) light (Excelitas) for 40 s to achieve photocrosslinking. The mold was subsequently disassembled, and the agarose microfibers were manually removed to leave hollow duct-like microchannels in the GelMA hydrogel.

To test the tri-culture system, GelMA solution mixed with 5×10^6 cells/mL of HepG2 cells was crosslinked and shaped to form 10 mm×12 mm×5 mm (length×width×height) structures containing alternant RBE- and HUVEC-populated microchannels (D=0.5 mm) generated by sacrificial bioprinting as described above. The coculture was performed for up to 9 days. To visualize the coculture, RBE-LifeAct-EGFP, HUVEC-LifeAct-RFP, and HepG2-Blue (cell tracker) were employed.

For drug screening and RNA sequencing, we wanted the results to only come from the tumor cells, and therefore, a detachable CCA-on-a-chip was designed. Based on sacrificial bioprinting, we first created a single 0.5-mm microchannel in a cuboid GelMA construct with a size of 2 mm×20 mm×2 mm. RBE or HUVEC suspension (1×10^7 cells/mL) was then injected to create functional microchannel components. The chips were cultured for

48 h, allowing the RBE cells and HUVECs to completely populate their respective microchannel surfaces. A GelMA solution was next mixed with 5×10^6/mL HepG2 cells, crosslinked, and shaped to a liver mode (circular section surface: D=3.5 cm). Finally, three RBE-functionalized components, three HUVEC-functionalized components, and one liver mode were assembled (totaling a size of 12 mm× 20 mm×2 mm). After coculturing for 2 or 7 days, RBE-functionalized components were isolated and collected for cytotoxicity tests or RNA isolation.

Assessment of mechanical properties of GelMA constructs

To assess the compressive moduli of the GelMA models, a universal testing system (Instron) was used. The samples were left in their original rectangular size, being 10 mm× 8 mm in area and approximately 4.3 mm in thickness. All measurements were performed at 0.4 mm/s. After loading each sample, five cycles from 0 to 10% were performed sequentially; after this test, the process was repeated to ensure that the results were reproducible until 10% strain was reached. Five more cycles were performed from 0 to 20% strain. Four final cycles were performed with increasing strain, starting at 0% strain and returning to 0% strain after each strain threshold: 10%, 20%, 30%, and 40%. The results from the final cycles (10% and 20%) were consistent with the individual trials at these strains. The compressive modulus was calculated as the slope of the stress–strain curve between 10% and 20% loading.

Observation of the diffusion of fluorescent peptides

To visualize whether the substances in the blood vessel could diffuse into the liver parenchyma, we synthesized linear peptides Arg-Gly-Asp-D-Tyr-Lys (RGDfK) that were bonded to fluorescein isothiocyanate (FITC) (Fig. S2a in Supplementary Information). After injecting RGDFK-FITC (2 mmol/L) into the microchannel (500 μm in diameter), snapshots of the diffusion of fluorescent peptides were automatically captured every 5 s with Zen software (Zeiss). Further diffusions of fluorescent peptides were semiquantitatively analyzed by fluorescent intensity mean values (IMVs) within and outside the microchannel (Fig. S2b in Supplementary Information).

Immunostaining

To show a clear image of adhesion to the microchannel walls and cellular crosstalk, dual-labeling immunostaining assays were undertaken. For HUVECs, mouse anti-human CD31 antibody (Abcam) and secondary antibody (goat anti-mouse IgG, Thermo Fisher) were used to yield a green colorimetric staining result. RBE channels were also stained green with rabbit anti-human cytokeratin (CK)-17 antibody (Thermo Fisher) and secondary antibody (goat anti-rabbit IgG, Thermo Fisher). Finally, F-actin in both samples was labeled in red using phalloidin (Thermo Fisher). To analyze the expression of P450 in HepG2 cells within CCA-on-a-chip, rabbit anti-human CYP3A4 (Thermo Fisher) and secondary antibody (goat anti-rabbit IgG, Thermo Fisher) were utilized. The stained samples were imaged using fluorescence and confocal microscopy.

Cell viability assay

Live/dead assays (LIVE/DEAD™ Viability/Cytotoxicity Kit, for mammalian cells, Thermo Fisher) were performed on the chips with seeded cells to quantify the viability of cultured cells in the selected GelMA hydrogels. Hydrogels were stained following the protocols described in the kit. The samples were taken to a fluorescence microscope. The assays were performed on 1, 3, 5, 7, and 9 days after seeding the cells.

On-chip antitumor drug screening

To test the performance of our model as a drug screening platform, a cytotoxicity assay was performed on the chip. For comparison, a 2D monoculture was also used. Both models were supplemented with increasing concentrations of cyclophosphamide (0, 1, 10, 100, 1000, 10,000 μg/mL). Viability was assessed 24 h later through a Cell Counting Kit-8 (CCK-8) test. Absorbance results (450-nm wavelength) were recorded at each concentration for each model. The viability values of the cells were compared to find statistically significant differences. The cell viability is calculated as follows:

$$\text{Cell viability} = \left[A(\text{Drug+}) - A(\text{Black})\right] / \left[A(\text{Drug}-) - A(\text{Black})\right] \times 100\%,$$

where A(Drug+) represents the optical density (OD) value of sample with cells, CCK-8, and drug, A(Drug−) represents the OD value of sample with cells, CCK-8, but without drug, and A(Black) represents the OD value of the sample with culture medium and CCK-8, but without cells.

RNA sequencing analyses

The chips were cultured for one week, allowing the cells to completely populate the microchannels. Then, RBE components were collected and soaked in TRIzol reagent for RNA isolation. Using RNA-seq technology (BGI Company), the expressed mRNA from each sample was converted to cDNA, and the fragments were counted after subsequent amplification. The magnified counts were used to compare gene expression levels between RBEs in 2D or 3D environments. The genes with significantly different mRNA levels between

the two groups were then defined as differentially expressed genes (DEGs), and their enriched gene ontologies (GO) and related pathways were identified through the Kyoto Encyclopedia of Genes and Genomes (KEGG) pathway and GO enrichment analyses.

Digital light processing-bioprinting of CCA-on-a-chip

To further demonstrate the possibility of producing complex CCA-on-a-chip structures, a digital light processing (DLP) bioprinter customized in the laboratory was used. A 3D computer model was sliced into 2D images using FormLab's open-source slicer (https://formlabs.com/blog/open-source-dlp-slicer/) and fed to the bioprinter's software to create the desired layer patterns. The bioprinter integrated a 450-nm-wavelength electronic laser, a digital micromirror device (DMD, TI DLP® LightCrafter™ 6500 Evaluation Module), a stepper motor (Nema 17, 1/8 microstepping configuration), a 10-cm leadscrew with shaft coupler, three optical lenses to focus the images into the vat, two aluminum front coated mirrors, two limit switch sensors, and an Arduino Mega board to control the system. A custom-made vat with an ultrathin transparent bottom was designed to fit the bioprinter setup. The building plate that lowered into the vat was built using acrylic and metallic rods.

To fabricate the DLP-bioprinting-based CCA-on-a-chip, a GelMA solution (40% (0.4 g/mL) Poly(ethylene glycol) diacrylate (PEGDA) or 5% (0.05 g/mL) porcine-H-GelMA) with 2-mmol/L tris-bipyridyl-ruthenium (II) hexahydrate (Ru) and 20-mmol/L sodium persulfate (SPS) (Advanced BioMatrix) was prepared as a bioink. Immediately before bioprinting, 5-μL/mL photoabsorber (Ponceau 4R, Sigma–Aldrich) was added. A total of 1×10^7/mL of cells were incorporated into the prepared bioinks. The models were fabricated according to a variety of predesigned patterns. Once each construct was bioprinted, it was taken from the build plate of the bioprinter and placed in PBS for 5 min to wash out the remaining uncrosslinked bioink prior to subsequent culture.

Image acquisition and processing

Immunofluorescence and brightfield micrographs of the cells were acquired with a fluorescence microscope (Eclipse, Nikon). Confocal images were acquired with a Zeiss confocal microscope (LSM880 with Airyscan, Carl Zeiss). ImageJ (National Institutes of Health) was used to merge the channels and render 3D reconstructions for confocal image stacks.

Statistical analyses

Statistical analyses were conducted by GraphPad Prism 8 (La Jolla, USA). Cell viability data are presented as the means±standard deviations (SDs). Significance tests were performed using Student's t-test. The results were considered significant at $p\leq0.05$ and $p\leq0.01$. Three samples were used for quantification in all groups, and at least five randomly selected images were taken per sample for analyses.

Results

CCA-on-a-chip models for better mimicking the 3D TME

CCA is the liver's primary tumor, occurring predominantly in the extrahepatic bile duct lumens; 60%–70% are in the perihilar region, approximately 25% in the distal ducts and the rest in the liver (Fig. 1a). Cholangiocytes, hepatic cells, and blood vessels have a very close relationship in anatomy and have commonly been identified to be involved in the pathophysiology of cholangiopathies (Fig. 1b). Due to the complexity of the disease and the need for better in vitro models to shed light on CCA occurrence, progression, and drug screening, our proposed model was improved from a monolayer 2D monoculture to a well-designed, biofabricated 3D CCA-on-a-chip coculture model made from an ECM-mimicking hydrogel microenvironment (Figs. 1c-i–iii).

While most CCA models are based on experiments using 2D cell cultures in vitro, they are limited by many factors, namely the lack of interactions between the cellular and extracellular environments, as well as the lack of physiologically relevant structures, dimensionality, and cell–cell communications (Fig. 1c-i). These disadvantages give impetus to the development of novel models that are able to more closely mimic the in vivo conditions. One such method is 3D culture. Using sacrificial bioprinting, we attempted to fabricate a CCA-on-a-chip model in which CCA (RBE) cells could 'xenograft' in an orthotopic manner and coexist with hepatic cells and vascular endotheliocytes (Fig. 1c-ii). Moreover, to achieve higher complexity and a more precise imitation of the tissue, DLP-based bioprinting was used to construct a well-designed biliary tree and vascular network in an effort to preliminarily introduce additional complexity into the CCA-on-a-chip platform (Fig. 1c-iii). These demonstrations suggest a potentially new strategy for constructing CCA models in vitro.

GelMA-based 3D functional microchannels to mimic blood vessels and bile ducts

We first fabricated functional microchannels for a CCA-on-a-chip model to mimic blood vessels and bile ducts using

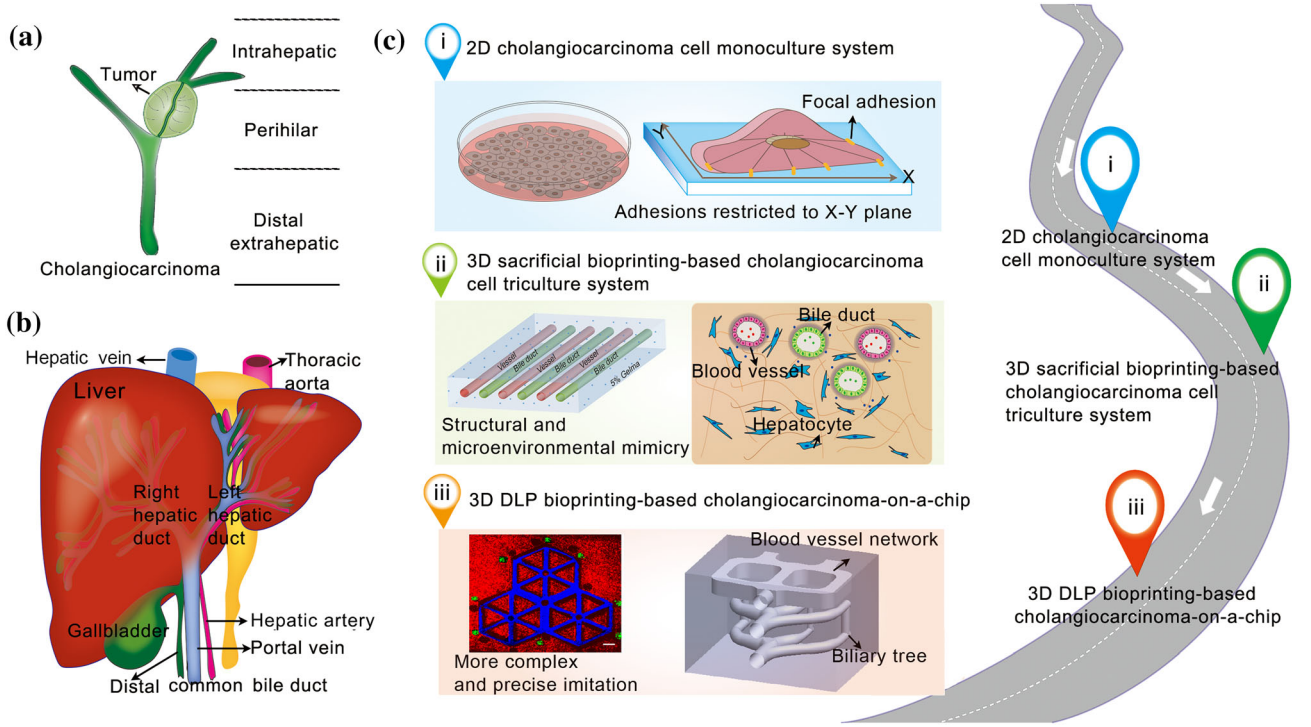

Fig. 1 Overview of the project. **a** Visual representation of cholangiocarcinoma (CCA) and its classification depending on its position along the biliary ducts. **b** Morphology of the liver, showcasing the structures that have hitherto rarely been replicated. **c** Progression of CCA model designs. (i) 2D presentation of the natural tissue. (ii) The 3D sacrificially bioprinted coculture mimics the multicellular system with higher confidence. The channels resemble the bile ducts, and the veins were present in the microenvironment. (iii) The 3D digital light processing (DLP)-bioprinted structure imitates the microenvironments more precisely. The sophistication of these structures favors cell growth, morphology, and pathology

sacrificial bioprinting. We chose GelMA as the bioink for 3D bioprinting the constructs because of its matrix metalloproteinase responsiveness and the presence of intrinsic cell-attaching peptide motifs [17, 18]. The models were fabricated by crosslinking GelMA inside dismantlable molds we designed, containing bioprinted agarose microfibers to produce the microchannels. The agarose microfibers used to create the microchannels had a diameter of 500 μm and were removed after photocrosslinking of GelMA, as we previously reported [19, 20]. Then, the CCA (RBE) cells and the endothelial cells (HUVECs) were seeded separately in those microchannels both at a concentration of 1×10^7 cells/mL. Once the cells were confluent within the microchannels, the biologically relevant microchannels were constructed. A schematic diagram of the preparation of the microchannels is depicted in Fig. 2a. A collection of designs is shown in Figs. 2b and 2c to illustrate the versatility in creating the microchannel molds. Acrylic molds were designed and laser-cut for preparing one or more microchannel-based molds depending on the requirements. By modifying the diameter of the agarose microfibers, the size of the microchannels could also be controlled in the range from approximately 300 μm to 1.6 mm but would not be limited in this range.

Another essential factor to consider when developing a relevant tissue model is the stiffness of the material where the cells will be cultured, as it plays a vital role in cellular behaviors and development. Thus, different sources and concentrations of GelMA were screened to select the one that best mimics the liver's mechanical properties and that best presents cellular compatibility. Figure S3a (Supplementary Information) shows that the cells were rounded and poorly attached in the microchannels made up of fish GelMA with a medium degree of methacryloyl modification (fish-medium-GelMA, or fish-M-GelMA) or a low concentration of fish-high-GelMA (fish-H-GelMA). However, RBE cells attached and spread with spindle or polygonal shapes in those made by porcine-M-GelMA and a high concentration of fish-H-GelMA 10% (0.1 g/mL). Further compressive modulus analyses revealed that high values were achieved for porcine-M-GelMA and high concentrations of fish-H-GelMA, which suggested the association of better cell adhesion with the higher stiffness of the underlying matrices (Figs. S3b and S3c in Supplementary Information). In other words, RBE cells would grow better on the surfaces of constructs with relatively high compressive moduli. Given that the typical value of liver stiffness is <6 kPa [21], the 5% (0.05 g/mL)

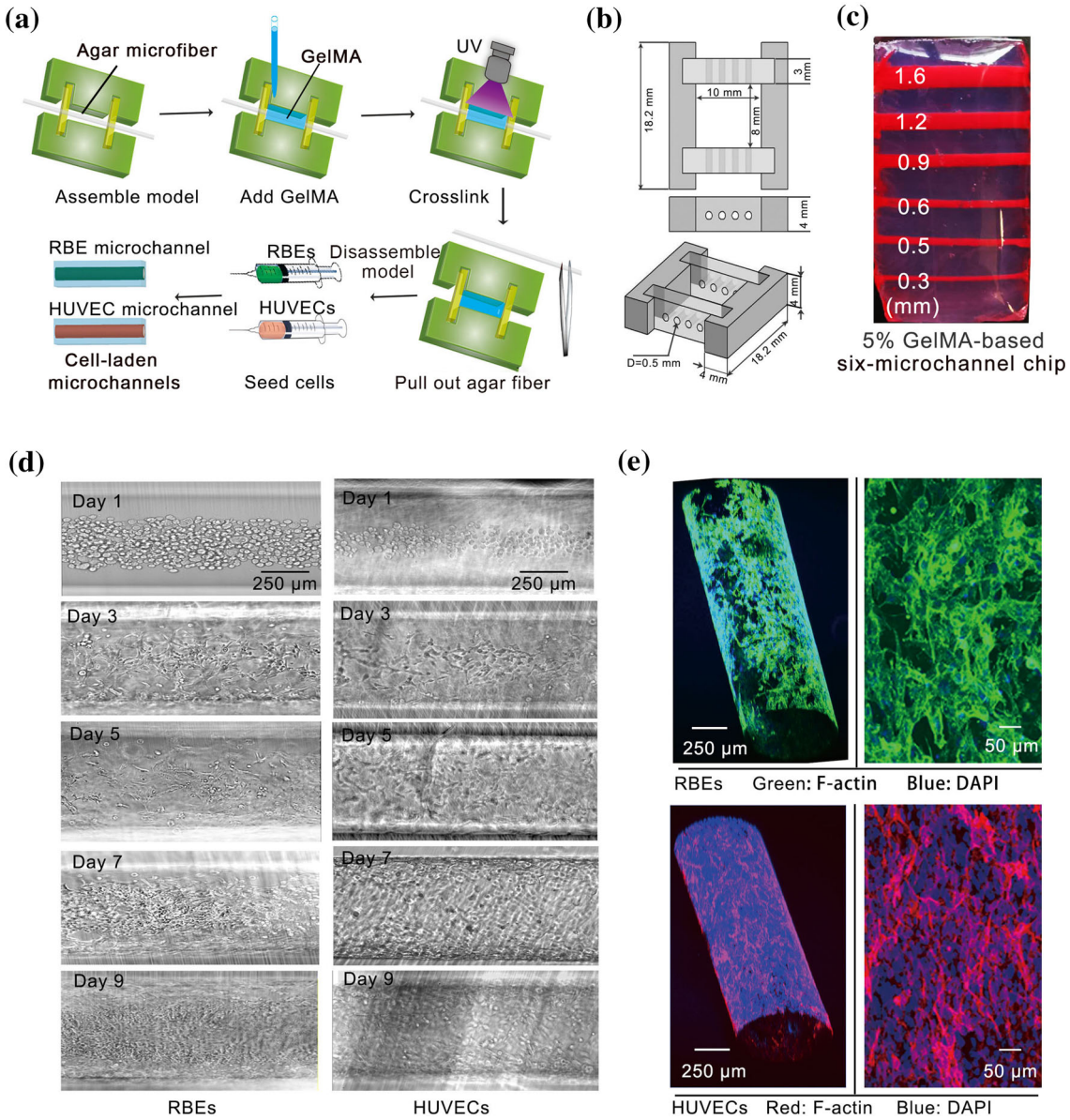

Fig. 2 Sacrificing bioprinting-enabled tubular microstructures were a viable culture environment for RBE cells and human umbilical vein endothelial cells (HUVECs). **a** Workflow diagram depicting the creation of gelatin methacryloyl (GelMA) microchannel constructs based on sacrificial bioprinting. **b** Schematic showing the dimensions of a four-channel chip mold. **c** Photograph showing the perfusion of microchannels with different diameters in a GelMA-based six-microchannel chip (D=0.3–1.6 mm). **d** Representative brightfield micrographs showing cell adhesion and spreading on the interior walls of the microchannels during the first 9 days of culture. **e** Confocal fluorescence micrographs of RBE cells and HUVECs growing along the interior walls of the microchannels after 9 days of culture, stained for F-actin and nuclei

porcine-M-GelMA was finally selected for subsequent model fabrication.

To validate the functional microchannels, we first evaluated cell growth in these GelMA-based microchannels. As observed in Fig. 2d, both RBE cells and HUVECs were rounded and clustered on the surfaces of the microchannels on the 1st day but could spread and proliferate in the following days, covering the entire surfaces of the microchannels by day 9. The 3D structurally intact cylindrical CCA and vascular microchannels were explicitly identified by F-actin and nuclear staining (Fig. 2e), which confirmed the optimal cytocompatibility of GelMA-based 3D microchannels to the cell types tested.

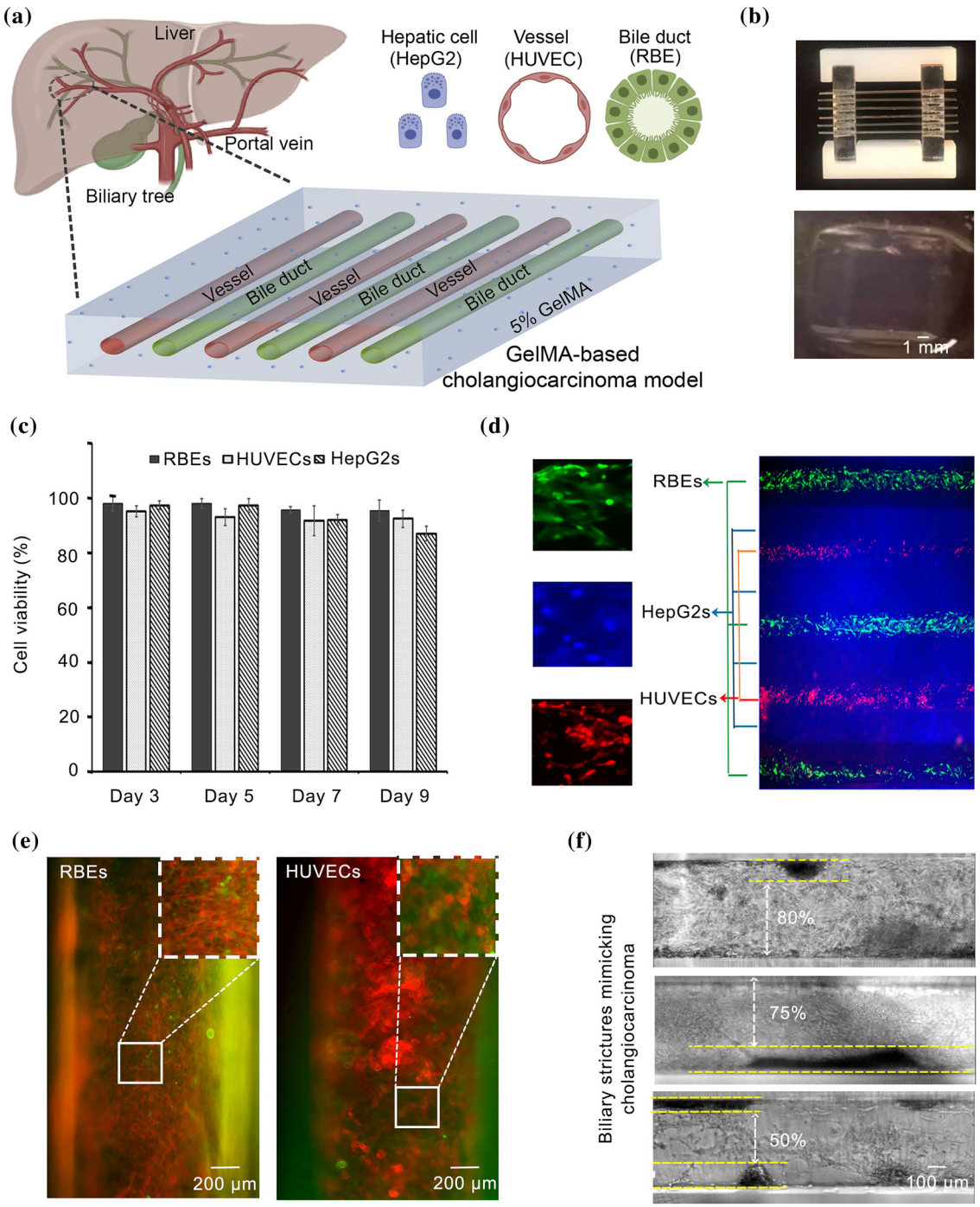

Fig. 3 Design, fabrication, and assessments of the cholangiocarcinoma (CCA)-on-a-chip tri-culture system. **a** Diagram showing the biomimetic capability of the chip model. The model recreates the interplay of bile ducts, blood vessels, and hepatic cells. **b** Top: photograph of the six-channel mold for creating the tri-culturing system produced by sacrificing bioprinting. Bottom: photograph showing the crosslinked gelatin methacryloyl (GelMA)-based CCA-on-a-chip model, in which HepG2 cells were directly encapsulated, and three RBE and human umbilical vein endothelial cell (HUVEC) microchannels were alternately embedded. **c** Cell viabilities during 9 days of culture as determined by a live/dead assay. **d** HUVEC-LifeAct-RFP (red), RBE-LifeAct-EGFP (green), and HepG2 marked by cell tracker (blue) were visible in alternating microchannels or within the GelMA construct by fluorescence microscopy imaging. **e** Confocal micrographs showing the specific markers of RBE cells and HUVECs. RBEs (CK17: green; F-actin: red); HUVECs (CD31: green; F-actin: red). **f** Micrographs showing the microchannel stricture in the CCA-on-a-chip model induced by cholangiocarcinoma-like hyperproliferation formed along the walls. Data are shown as the means±standard deviations (SDs)

Multicellular CCA-on-a-chip developed CCA hyperproliferation-induced stenosis of the bile duct

Based on the functional microchannels, we further designed and constructed a multicellular 3D CCA-on-a-chip model that allowed the coculture of RBE cells, hepatocyte-like cells (HepG2), and vascular endotheliocytes (HUVECs). As shown in Fig. 3a, within the liver, the biliary tree runs along the portal vein branches of the hepatic artery, giving rise to a close anatomic association classically represented in the liver microarchitecture. To maximally replicate the local microenvironment and model the cellular interactions of CCA, we fabricated a six-microchannel CCA-on-a-chip tri-culture system (Fig. 3b). In these chips, HepG2 cells were embedded in a GelMA-based matrix to mimic the liver parenchyma. To simulate the bile duct and vascularization, three RBE-functionalized microchannels and three HUVEC-functionalized microchannels were embedded in an alternating fashion in each chip, allowing for possible cellular crosstalk.

Considering that different cell types were present in the tri-culture, the nutritional medium had to be adjusted to ensure efficient growth. First, when RBE/HUVEC/HepG2 culture media were used at a 1:1:1 volume ratio, HUVECs were dying after 72 h. To support the growth of HUVECs, VEGF was additionally included in the coculture system at a concentration of 10 ng/mL. As shown in Fig. 3c, the viability assay indicated that with the addition of VEGF, more than 90% of HUVECs remained viable and could attach to the microchannels. Moreover, over 90% of the RBE cells and HepG2 cells survived and proliferated in the GelMA matrix throughout the entire tri-culture period of up to 9 days. Thus, VEGF-supplemented tri-culture medium was used for subsequent experiments.

To easily distinguish and visualize the cells in the model, we performed lentivirus transfections of fluorescent proteins. HUVECs were transfected with LifeAct-RFP (HUVEC-LifeAct-RFP) and RBEs with LifeAct-EGFP (RBE-LifeAct-EGFP) (Figs. S2a and S2b, respectively, in Supplementary Information). To monitor HepG2 cell distribution, they were marked with CellTracker™ Blue (HepG2-Blue) immediately before model fabrication. As shown in Fig. S2c (Supplementary Information), HepG2-Blue cells grew and spread after 48 h of model construction. After 4 days of coculture (Fig. 3d), the HUVECs-LifeAct-RFP and RBE-LifeAct-EGFP cells grew well in separated and alternating microchannels, and the HepG2-Blue cells were rounded, scattered, and distributed in the surrounding GelMA matrix. Further dual-labeling immunofluorescence imaging for F-actin and CK17 (Fig. 3e) suggested that the specific marker of epithelial cells, CK17 (green), was highly expressed in RBE cells (non-EGFP), and F-actin staining (red) revealed tight cell–cell connections between the RBEs. In addition, CD31 (green), as an endothelial cell marker, was highly expressed in HUVECs, indicating the favorable functions of these cells. In conclusion, this six-microchannel-based CCA-on-a-chip model allowed for cellular communications for each of the three cell lines and reconstructed the particular microstructure that characterized local CCA to a good extent.

More interestingly, hyperproliferation of RBE cells in the CCA-on-a-chip model was observed when cultured for 9 days (Fig. 3f), which implied that the microstructure and microenvironment of these models were beneficial for CCA cell growth and tumor hyperplasia. This evidence suggested that the microchannel structure accurately represented the biliary stricture, particularly in CCA cases, which cannot be recapitulated with conventional 2D cultures.

Sensitization of CCA cells to cyclophosphamide (CPA) induced by 3D CCA-on-a-chip tri-culture and 2D monoculture models

CPA, a widely used oxazaphosphorine anticancer prodrug, is easily absorbed but is inactive until it is metabolized by mixed-function oxidase enzymes (cytochrome P450 system) in the liver, which yields phosphoramide mustard and acrolein that alkylate DNAs and proteins, respectively (Fig. 4a) [22].

To compare the 2D and 3D screening models and demonstrate the superiority of the CCA-on-a-chip model in drug screening, CPA concentrations ranging from 1 μg/mL to 10 mg/mL were employed for a drug toxicity test. To facilitate drug screening, a slightly modified CCA-on-a-chip configuration was employed. As shown in Fig. 4b, RBE- and HUVEC-functionalized microchannels and the liver model with a cuboid depression in the middle were assembled to form a complete model. Further analyses of the diffusion of fluorescent peptides showed that substances in the vascular microchannels were able to diffuse into the liver parenchyma over time (Fig. S2 in Supplementary Information).

Cytotoxicity tests were conducted in a 6-well plate for 24 h, followed by a PrestoBlue test on the RBE-functionalized microchannels. As expected, the toxicity of CPA to 2D-cultured RBEs was relatively low, even at a concentration of 1 mg/mL. However, in the CCA-on-a-chip model, cytotoxicity was shown to be dependent on the concentration; with increasing drug concentration, increasing cell death was observed (Fig. 4c). Notably, after CPA treatment for 24 h, CYP3A4 expression in HepG2 cells was found to be dramatically higher than that in untreated HepG2 cells (Fig. S4 in Supplementary Information). This phenomenon infers that the neighboring HepG2 cells in the coculture system probably converted CPA to the active form aldophosphamide by P450 (CYP3A4) [23], which traditionally could only be verified by in vivo models and was hard to assay in 2D monocultures, although not entirely impossible. Thus,

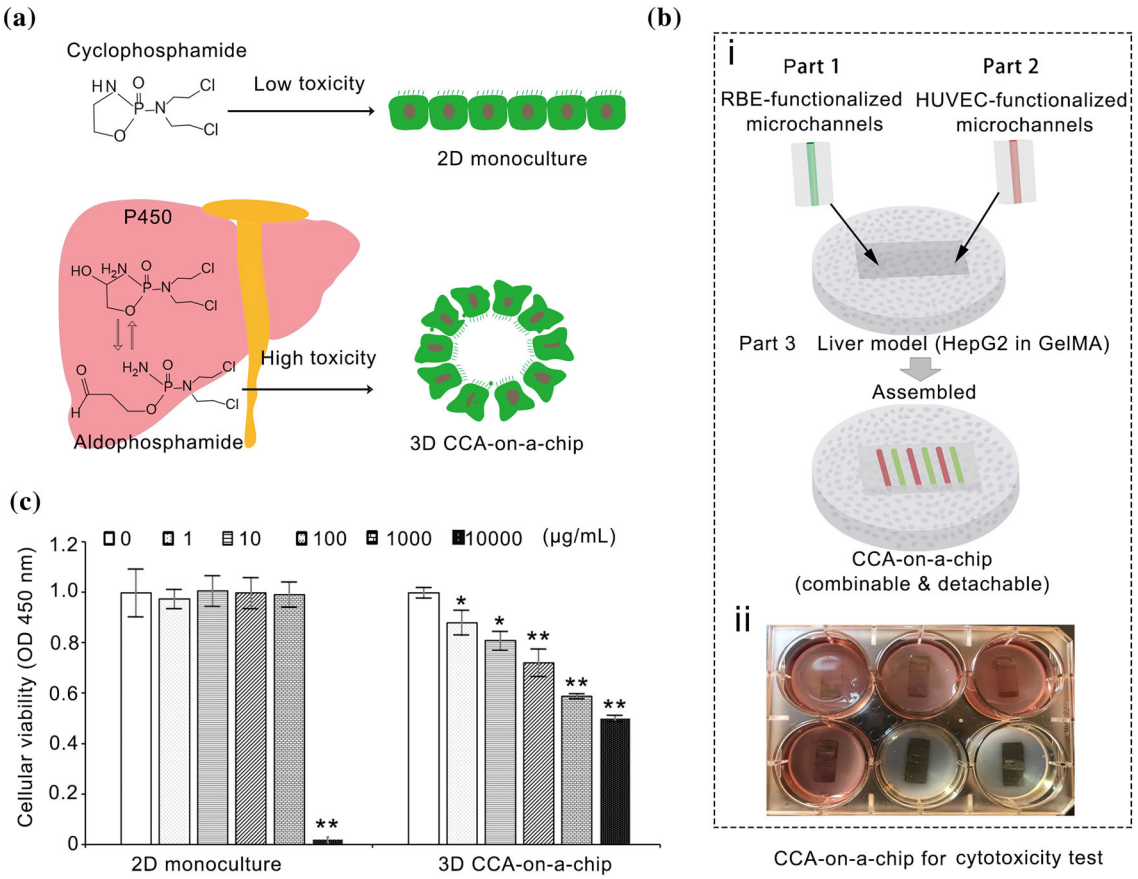

Fig. 4 Application of antitumor drug screening based on the 2D monoculture and the 3D cholangiocarcinoma (CCA)-on-a-chip models. **a** Schematic diagram showing the advantage of the 3D CCA-on-a-chip model. As a low-toxicity prodrug, cyclophosphamide (CPA) can be converted to highly toxic aldophosphamide, which is dependent on cytochrome P450 metabolism in cocultured liver cells in the 3D CCA-on-a-chip model. However, it does not occur in the 2D monoculture. **b** Schematic diagram showing the modified 3D tri-culture CCA-on-a-chip model for antitumor drug screening. (i) Three RBE or three human umbilical vein endothelial cell (HUVEC)-functionalized microchannels were independently assembled within a larger HepG2-embedded liver construct for assembling the CCA-on-a-chip. (ii) Tri-culture of the assembled 3D CCA-on-a-chip model for cytotoxic screening. **c** Cytotoxicity analyses of CPA in 2D monoculture and 3D CCA-on-a-chip models by CCK-8 assay. Data are shown as the means±standard deviations (SDs). *p<0.05 and **p<0.01 versus the corresponding 0 μg/mL groups

this study potentially brings us a promotion model to search for new antitumor medicines and new treatment strategies.

Differential gene expression induced by CCA-on-a-chip and 2D models

In addition to the applications for drug screening, the 3D CCA-on-a-chip model may further help improve the understanding of cancer biology by more accurately replicating the genetic profiles of cancer cells/tissues [24]. Herein, we performed RNA-seq on the RBEs for 2D monoculture as well as in tri-culture in the detachable CCA-on-a-chip model to evaluate the differences in gene expression and identify the major signaling pathways that were differentially regulated. The results showed a certain degree of differences between the two conditions, with a Spearman rank correlation coefficient of 0.77 (Fig. 5a). The volcano plot indicated that 4193 DEGs (|$\log_2$(fold change)|=0.58, Q value<0.05) were labeled on the map (Fig. 5b).

We further performed KEGG pathway/GO enrichment analyses and found that the DEGs were enriched in 20 major signaling pathways. We identified 166 DEGs that corresponded to cancer pathways (Fig. 6a). We analyzed the p53 pathway, a well-known tumorigenesis-related pathway [25], to further understand the importance of our CCA-on-a-chip model. As expected, 31 DEGs were enriched in this pathway, and 28 genes were downregulated compared to the traditional 2D monoculture, which was strong evidence that the p53 signaling pathway was universally downregulated in the 3D CCA-on-a-chip model. Inactivation of p53 and repression of phosphatase and tensin homolog (PTEN) have been

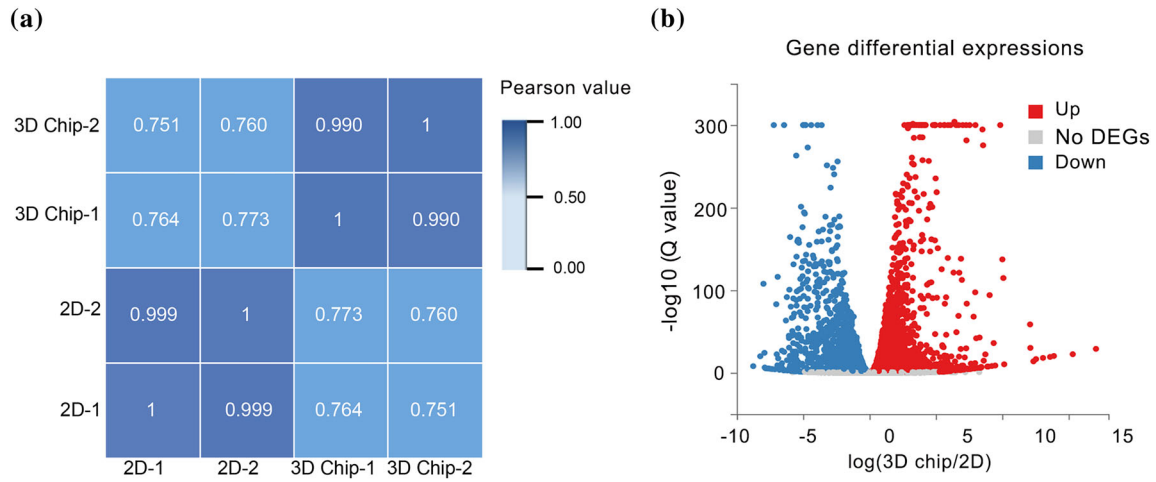

Fig. 5 Analysis of global gene expression of the RBE by RNA-Seq. **a** Global gene expression correlation study of the RBEs in 2D monoculture and 3D cholangiocarcinoma (CCA)-on-a-chip coculture models. **b** Volcano plot of statistically significant differentially expressed genes at $Q<0.05$ identified from the RNA-Seq libraries of the RBEs in 2D monoculture and 3D CCA-on-a-chip coculture models

proved to play crucial roles in tumorigenesis of CCA and malignant phenotypes of iCCA cells [25–28]. Therefore, it is of great significance to downregulate p53 and PTEN in our 3D CCA-on-a-chip tri-culture system. Although there was no clear evidence of a link to tumorigenesis of CCA, the only other 3 genes that were upregulated were highly relevant, including cell cycle inhibitors (growth arrest and DNA damage-inducible protein: GADD45, growth arrest and DNA damage-inducible protein: P21) [29] and IGF-1 pathway inhibitors (insulin-like growth factor-binding protein 3: IGF-BP3) [30] (Fig. 6b). The significant differences in tumor-associated pathways suggested that the failure of 2D monoculture drug screening models could partly be attributed to differential gene expression induced by insufficient recapitulation of the TME.

More sophisticated CCA-on-a-chip models fabricated by DLP bioprinting

DLP-based 3D bioprinting, which often uses a DMD to produce dynamic photomasks, enables rapid and selective solidification of the bioink to form well-defined, crosslinked 3D constructs containing more complex structures than those that can be attained with sacrificial bioprinting (Fig. S5 in Supplementary Information) [31–37]. We attempted two proof-of-concept demonstrations in generating CCA-on-a-chip models that better mimicked the native architecture using DLP bioprinting despite less biology demonstrated in this work.

In the first example, we encapsulated fluorescently labeled HepG2 cells (red), HUVECs (blue), and RBE cells (green) in complementary patterns that resembled the hepatic lobule structure by photopolymerizing the hydrogel matrices in a planar manner. Three complementary patterns as binary digital masks were designed to resemble the anatomical features of the tissue (Fig. 7a). To spatially pattern multiple types of cells, the masks were applied in a three-step sequential manner to create a first layer of hepatic cells, followed by a second and third complementary layer of vascular and bile ducts [37]. The procedure successfully patterned the three types of cells into a liver lobule-like structure (Fig. 7b).

Although this three-layer design demonstrated the feasibility of potential interactions among the three cell types, we sought to further introduce additional structural features and microchannels into a bioinspired, truly 3D model of CCA. For this purpose, we embedded structurally and functionally separated microchannels in the model. As shown in Fig. 7c, the microchannels of the vessels mimicked the spatial anatomical structure of the dual blood supply in the liver. In addition, the design of the double-layer branching duct tree was inspired by the native structure of the biliary tree. Separately, the intertwined vascular and bile ducts were also designed and printed, as shown in Figs. 7d and 7e. The models measured 6 mm×6 mm, with a thickness of 5 mm. The diameters of the microchannels were as small as 200–500 μm (Fig. 7f). Subsequent perfusion further confirmed the interconnection of these microchannels (Fig. 7g). These models suggested improved structural resemblance to the complex structure of the native CCA, where afferent blood vessels and bile ducts traverse the liver, and would be an appropriate tool for CCA research and screening of therapies in the future with further optimization.

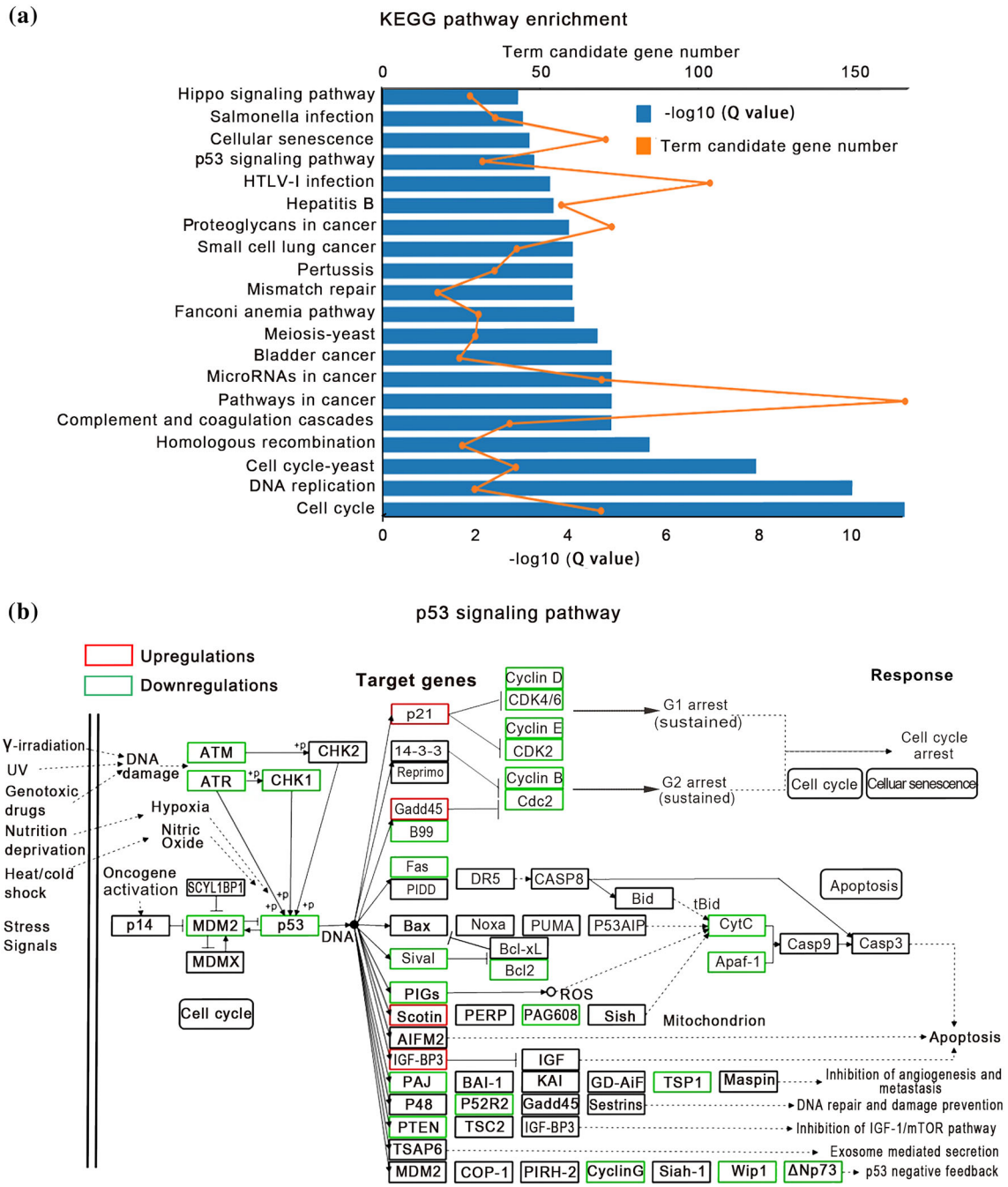

Fig. 6 Kyoto Encyclopedia of Genes and Genomes (KEGG) pathway analyses between 2D monoculture and 3D cholangiocarcinoma (CCA)-on-a-chip tri-culture models based on RNA-seq. **a** The main KEGG pathways where over 500 changed genes resided. **b** Differential gene expression in the p53 signaling pathway. Red frames: upregulation in the 3D CCA-on-a-chip tri-culture model compared to the 2D monoculture; green frames: downregulation in the 3D CCA-on-a-chip tri-culture model compared to the 2D monoculture

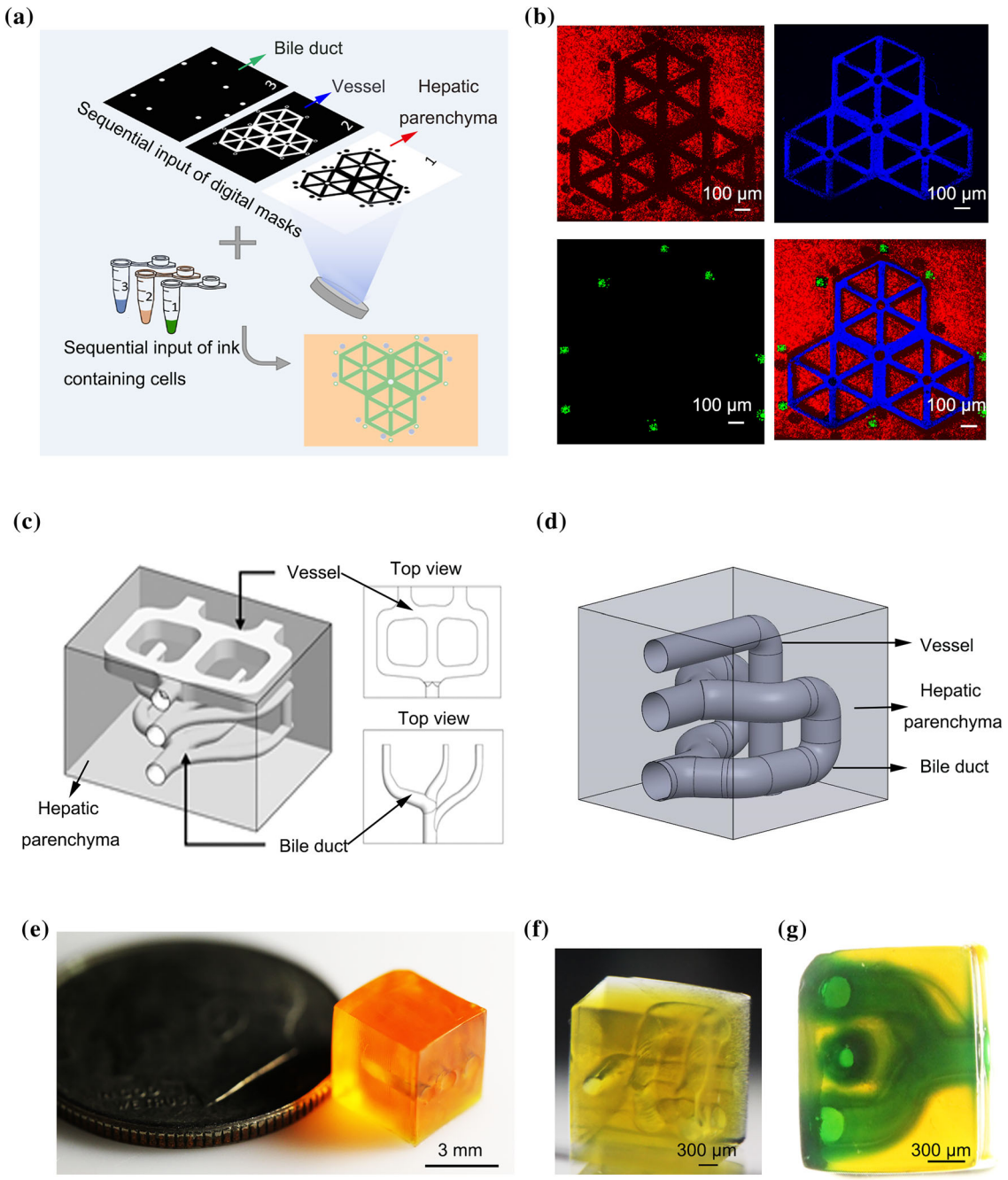

Fig. 7 Proof-of-concept digital light processing (DLP) (bio)printing-based cholangiocarcinoma (CCA)-on-a-chip models. **a** Schematic diagram of a three-step approach in which HepG2 cells were patterned by the first digital mask followed by the patterning of human umbilical vein endothelial cells (HUVECs) and RBE cells using the second and third digital masks, respectively. Three different bioinks with fluorescently labeled cells facilitated the observation of the bioprinted CCA-on-a-chip construct. **b** Fluorescence micrographs showing patterns of fluorescently labeled HepG2 cells (red), RBEs (green) and HUVECs (blue) in 5% (0.05 g/mL) gelatin methacryloyl (GelMA), on day 0. **c** Computer model of the hierarchic lumen structure: both blood vessels (top) and bile ducts (bottom) were separately layered in this model. **d** Computer model of the entwined lumen structure: bile ducts (Y shape) and blood vessels (L shape) were intertwined in this model. **e** Size of the bioprinted 3D CCA model compared with a US quarter. **f** Top view of the printed structure. **g** Photograph of the construct with open microchannels, which were perfused with a green food dye to demonstrate microchannel connectivity

Discussion

CCA-on-a-chip reproduced the microenvironment and microstructure of CCA to a decent extent

The CCA microenvironment is a complex, multicellular functional compartment that may profoundly affect mechanosensing as well as other responses and consequently the proliferative and invasive abilities of residing cancer cells [38]. Therefore, tumor models that can mimic the realistic situation in vivo outside the body are of great significance for studies of tumor biology and drug discovery.

The dialogue between CCA cells and the ECM is of remarkable importance in the native pathophysiological conditions that affect cancer progression and ECM remodeling [39]. In particular, matrix viscoelasticity plays a crucial role in these dynamic communications; it is not only required for the tumor to be able to displace the host tissue and grow in size but also contributes to cell-ECM interactions and can promote cancer cell invasion to surrounding tissues [40]. Furthermore, matrix properties have been reported to be coupled with the intracellular glutamine content, thus affecting cancer cell proliferation [41]. In addition, ECM stiffness is linked to the induction of epithelial-to-mesenchymal transition (EMT) and promotes angiogenesis, altering normal vasculature integrity to mimic cancer-associated vasculature [42, 43]. Herein, for the CCA model, different origins and concentrations of GelMA were evaluated in terms of their cytocompatibility and compressive moduli. As shown in Fig. S3 (Supplementary Information), the 5% crosslinked porcine-M-GelMA, applied in the CCA-on-a-chip model, demonstrated a stiffness similar to that of the native liver, which possibly contributed to the biomimetic cellular gene expression and drug responses associated with the ECM microenvironment.

In addition to stiffness, GelMA hydrogels closely resemble the essential 3D properties of the native ECM due to their intrinsic cell-instructive properties and the presence of matrix metalloproteinase-responsive motifs [44]. Thus, encapsulated hepatocyte-like cells as well as CCA cells and endotheliocytes attached onto the inner surfaces of the microchannels, achieving favorable cell viability (Fig. 2d).

The multicellular microenvironment and luminal microstructures are also vital anatomical and pathophysiological features of CCA. Unlike other 3D models [45, 46], in this study, our CCA-on-a-chip model featuring an embedded lumen-like microstructure, which resembled interlacing vessels and bile ducts, was designed and bioprinted to mimic the in vivo CCA to a good extent. The model combined photocurable GelMA with CCA cells, vascular endotheliocytes, and hepatocyte-like cells. Through the simulation of the microenvironment and the microstructures, it was possible to observe the RBE cells attaching to the surfaces of the GelMA-embedded microchannels (Fig. 2e) overgrowing in a thickening manner, generating bile duct stenosis (Fig. 3f), which was expected to be analogous to the in vivo configuration [27].

3D bioprinting techniques facilitated the fabrication of CCA-on-a-chip models

Recapitulating human CCA in a physiologically relevant 3D multicellular environment is the ultimate goal of in vitro CCA modeling. For this reason, efforts have been exerted to achieve in vivo mimicry through various biofabrication technologies, which would allow more accurate studies of tumorigenesis than conventional 2D cultures and the establishment of personalized therapy in the future. For instance, intrahepatic CCA cells isolated from patients were bioprinted using a hydrogel composed of gelatin-alginate-Matrigel into predesigned grid architectures, which put forwards an appealing method for personalizable therapy [47]. Furthermore, bioprinting has a unique advantage in integrating the microchannel structure with tumor models. Our previous work confirmed that blood or lymphatic vascular structures could be achieved via sacrificial bioprinting, where microchannels could first be formed within the hydrogel matrix through selective removal of the bioprinted fugitive bioinks and then seeded with vascular or lymphatic endothelial cells onto the interior surfaces [19]. Additionally, bioprinting could enable the fabrication of single- or multi-layered hollow tubular structures in a single step, which would be an enabling model of standalone vessels when cellularized [7, 48]. Finally, high-resolution patterns could also be formed to model the dendritic vascularization of organs [17].

One of the main difficulties in currently reported 3D CCA models, however, is the general lack of vascular networks and bile ducts, which play crucial roles in CCA progression. We designed and developed a CCA-on-a-chip model for gene expression and drug screening analyses through a combination of sacrificial bioprinting and microfluidic chip devices (Fig. 3) [16]. Endothelial cells and CCA cells were seeded to form tubular microvessels and bile ducts embedded in a surrounding matrix of hepatocyte-like cells, which is a unique configuration not reported before. With a medium optimized for tri-culture, the CCA cells were observed to display hyperproliferation in a 3D thickening manner, expectantly analogous to the in vivo malignant biliary stenosis [27], which demonstrated a close representation of the realistic anatomical condition of CCA, allowing for a complex interplay of structural and biological elements that impact cellular responses.

Moreover, as tentatively explored in the work, DLP-based 3D bioprinting was used to build more sophisticated architectures than sacrificial bioprinting. As shown in Figs. 7a and

7b, DMD-based DLP 3D bioprinting granted flexibility in fabrication and thus facilitated the process of liver lobule pattern design [23, 33, 34]. The three complementary hexagonal and dotted patterns resembled the native microarchitecture, enabling intimate contact at the pattern interfaces and potentially permitting local paracrine interactions between CCA cells and neighboring cells. Carefully adjusting the bioprinting parameters further allowed us to achieve the fabrication of volumetric constructs with complex embedded microstructures of tubular vessels and the biliary tree (Figs. 7c–7g). Of note, while it is rational to postulate that the DLP-bioprinted CCA-on-a-chip model would also show superior cellular behaviors and drug responses than 2D cultures similar to the case of the model produced by sacrificial bioprinting, this hypothesis still requires validation in the future with additional studies on this specific model.

Application of the CCA-on-a-chip model in drug screening

One major objective in tumor-mimicking models is to understand tumor biology related to metastasis mechanisms and the tumor microenvironment, which could support the development of new anticancer drugs and treatment options [49]. However, previously established drug screening models, namely monoculture models and PDX/PDOX mouse models, have various deficiencies in their utilities. On the one hand, a 2D monolayer monoculture lacks the necessary architecture and microenvironment to simulate cell responses correctly; they have limitations in cell interactions, require morphology improvements to represent an actual disease, and have oversimplified architecture, which negatively impacts cell growth, gene expression, and drug responses [24, 50]. On the other hand, PDX models, while more physiologically accurate, are complex in handling, expensive, and time-consuming, which in turn makes them oftentimes inconvenient for functional studies [51].

Biofabricated 3D CCA models, with their capacity to simulate cell responses while remaining relatively easy to produce, represent a class of promising in vitro platforms for antitumor drug screening [49]. With the proper mechanical and biochemical cues in place, our bioprinted, chip-based model proved to be a decent recreation of the native CCA. As shown in Figs. 5 and 6, significant differences in the gene expression of RBE cells were exhibited between the 2D monoculture and our 3D CCA-on-a-chip coculture configuration, especially in the p53 signaling pathway. p53 is the most commonly mutated tumor suppressor gene and has been implicated in CCA development [27]. The inhibition of the p53 signaling pathway in our 3D CCA-on-a-chip model indicated that this high-content model would probably be a potential tool to uncover the underlying tumorigenesis as well.

More promisingly, the CCA-on-a-chip model displayed an in vivo-like response to chemotherapeutic agents (Fig. 4). Our results confirmed that RBE cells grown in the chips along with other auxiliary cell types showed more sensitivity to the antitumor prodrug CPA than those grown in a 2D monoculture. This phenomenon was due to drug biotransformation by neighboring functional hepatic-like cells in our 3D tri-culture configuration. In the future, combination with patient-derived tumor cells will likely endow the CCA-on-a-chip model with enhanced potential in personalized medicine.

Conclusions

In conclusion, a series of 3D CCA-on-a-chip tri-culture models were created via sacrificial or DLP-based (bio)printing, which were demonstrated to mimic the native CCA conditions to a good extent as a result of their complex interplay of structural and biological elements that impact cellular behaviors and responses to antitumor compounds. This model represents a potential personalized screening method that does not compromise accuracy, cost, or ease of use when further optimized.

Supplementary Information The online version contains supplementary material available at https://doi.org/10.1007/s42242-022-00229-9.

Acknowledgements The authors acknowledge support by the Brigham Research Institute.

Author contributions QL and YSZ devised the project. QL, LSM, CV, IA, and MV conducted designs and testing of 3D CCA-on-a-chip models, processed the experimental data, and performed the analyses. QL, LSM, SY, WL, and JL prepared the GelMA. YS tested the expression of CYP3A4 in the 3D culture model and the 2D RBE model. HW performed additional diffusion test. QL, LSM, CV, and YSZ drafted the manuscript. QL and YSZ revised the manuscript. LX participated in the review and editing of the manuscript.

Declarations

Conflict of interest YSZ consults for Allevi by 3D Systems, and sits on the scientific advisory board and holds options of Xellar, both of which however, did not participate in or bias the work.

Ethical approval This study does not contain any studies with human or animal subjects performed by any of the authors.

References

1. Olaizola P, Perugorria MJ, Banales JM (2018) Toward personalized medicine for intrahepatic cholangiocarcinoma: pharmacogenomic stratification of patients. Hepatology 68:811–814. https://doi.org/10.1002/hep.29830
2. Dvir K, Galarza Fortuna GM, Cortez N et al (2020) Advances in cholangiocarcinoma treatment in the personalized medicine

era. Open J Hepatol 2(1):006–008. https://doi.org/10.17352/ojh.000004
3. Pauli C, Hopkins BD, Prandi D et al (2017) Personalized in vitro and in vivo cancer models to guide precision medicine. Cancer Discov 7(5):462–477. https://doi.org/10.1158/2159-8290.CD-16-1154
4. Fabris L, Sato K, Alpini G et al (2021) The tumor microenvironment in cholangiocarcinoma progression. Hepatology 73(S1):75–85. https://doi.org/10.1002/hep.31410
5. Menon JU (2018) 3D tumor models for cancer drug discovery: current status and outlook. J Med Ther 2(3):1–2. https://doi.org/10.15761/JMT.1000137
6. Pompili L, Porru M, Caruso C et al (2016) Patient-derived xenografts: a relevant preclinical model for drug development. J Exp Clin Cancer Res 35:189. https://doi.org/10.1186/s13046-016-0462-4
7. Cao X, Ashfaq R, Cheng F et al (2019) A tumor-on-a-chip system with bioprinted blood and lymphatic vessel pair. Adv Funct Mater 29(31):1807173. https://doi.org/10.1002/adfm.201807173
8. Trujillo-de Santiago G, Flores-Garza BG, Tavares-Negrete JA et al (2019) The tumor-on-chip: recent advances in the development of microfluidic systems to recapitulate the physiology of solid tumors. Materials 12(18):2945. https://doi.org/10.3390/ma12182945
9. Li J, Parra-Cantu C, Wang Z et al (2020) Improving bioprinted volumetric tumor microenvironments in vitro. Trends Cancer 6(9):745–756. https://doi.org/10.1016/j.trecan.2020.06.002
10. Zhang YS, Zhang YN, Zhang WJ (2017) Cancer-on-a-chip systems at the frontier of nanomedicine. Drug Discov Today 22(9):1392–1399. https://doi.org/10.1016/j.drudis.2017.03.011
11. Kaemmerer E, Melchels FPW, Holzapfel BM et al (2014) Gelatine methacrylamide-based hydrogels: an alternative three-dimensional cancer cell culture system. Acta Biomater 10(6):2551–2562. https://doi.org/10.1016/j.actbio.2014.02.035
12. Park KM, Lewis D, Gerecht S (2017) Bioinspired hydrogels to engineer cancer microenvironments. Ann Rev Biomed Eng 19:109–133. https://doi.org/10.1146/annurev-bioeng-071516-044619
13. Ching T, Toh YC, Hashimoto M et al (2021) Bridging the academia-to-industry gap: organ-on-a-chip platforms for safety and toxicology assessment. Trends Pharmacol Sci 42(9):715–728. https://doi.org/10.1016/j.tips.2021.05.007
14. Sharifi F, Yesil-Celiktas O, Kazan A et al (2020) A hepatocellular carcinoma–bone metastasis-on-a-chip model for studying thymoquinone-loaded anticancer nanoparticles. Bio-Des Manuf 3:189–202. https://doi.org/10.1007/s42242-020-00074-8
15. Zhang YS, Aleman J, Shin SR et al (2017) Multisensor-integrated organs-on-chips platform for automated and continual in situ monitoring of organoid behaviors. Proc Natl Acad Sci USA 114(12):E2293–E2302. https://doi.org/10.1073/pnas.1612906114
16. Zhang YS, Khademhosseini A (2020) Engineering in vitro human tissue models through bio-design and manufacturing. Bio-Des Manuf 3:155–159. https://doi.org/10.1007/s42242-020-00080-w
17. Ying GL, Jiang N, Yu C et al (2018) Three-dimensional bioprinting of gelatin methacryloyl (GelMA). Bio-Des Manuf 1:215–224. https://doi.org/10.1007/s42242-018-0028-8
18. Ma HL, Li W, Wang M, Varanda LC, Perussi JR, Zhang YS, Carrilho E (2022) In vitro 3D malignant melanoma model for the evaluation of hypericin-loaded oil-in-water microemulsion in photodynamic therapy. Bio-Des Manuf *5*, 660–673.
19. Liu T, Liu Q, Anaya I et al (2021) Investigating lymphangiogenesis in a sacrificially bioprinted volumetric model of breast tumor tissue. Methods 190:72–79. https://doi.org/10.1016/j.ymeth.2020.04.003
20. Duchamp M, Liu T, van Genderen AM et al (2019) Sacrificial bioprinting of a mammary ductal carcinoma model. Biotechnol J 14(10):1700703. https://doi.org/10.1002/biot.201700703
21. Mueller S, Sandrin L (2010) Liver stiffness: a novel parameter for the diagnosis of liver disease. Hepatic Med Evid Res 2:49–67. https://doi.org/10.2147/hmer.s7394
22. Greco O, Dachs GU (2001) Gene directed enzyme/prodrug therapy of cancer: historical appraisal and future prospectives. J Cell Physiol 187(1):22–36. https://doi.org/10.1002/1097-4652(2001)9999:9999%3c::AID-JCP1060%3e3.0.CO;2-H
23. Coban MA, Morrison J, Maharjan S et al (2021) Attacking COVID-19 progression using multi-drug therapy for synergetic target engagement. Biomolecules 11(6):787. https://doi.org/10.3390/biom11060787
24. Kapałczyńska M, Kolenda T, Przybyła W et al (2016) 2D and 3D cell cultures: a comparison of different types of cancer cell cultures. Arch Med Sci 14(4):910–919. https://doi.org/10.5114/aoms.2016.63743
25. El Khatib M, Bozko P, Palagani V et al (2013) Activation of Notch signaling is required for cholangiocarcinoma progression and is enhanced by inactivation of p53 in vivo. PLoS ONE 8(10):e77433. https://doi.org/10.1371/journal.pone.0077433
26. Maroni L, Pierantonelli I, Banales JM et al (2012) The significance of genetics for cholangiocarcinoma development. Ann Transl Med 1(3):28–45. https://doi.org/10.3978/j.issn.2305-5839.2012.10.04
27. Banales JM, Marin JJG, Lamarca A et al (2020) Cholangiocarcinoma 2020: the next horizon in mechanisms and management. Nat Rev Gastroenterol Hepatol 17:557–588. https://doi.org/10.1038/s41575-020-0310-z
28. Wang LJ, He CC, Sui X et al (2015) MiR-21 promotes intrahepatic cholangiocarcinoma proliferation and growth in vitro and in vivo by targeting PTPN14 and PTEN. Oncotarget 6:5932–5946. https://doi.org/10.18632/oncotarget.3465
29. Jin X, Liu XG, Zhang Z et al (2018) Identification of key pathways and genes in lung carcinogenesis. Oncol Lett 16(4):4185–4192. https://doi.org/10.3892/ol.2018.9203
30. Ranke MB (2015) Insulin-like growth factor binding-protein-3 (IGFBP-3). Best Pract Res Clin Endocrinol Metab 29(5):701–711. https://doi.org/10.1016/j.beem.2015.06.003
31. Wang M, Li W, Mille LS et al (2021) Digital light processing based bioprinting with composable gradients. Adv Mater 34(1):2107038. https://doi.org/10.1002/adma.202107038
32. Li W, Wang M, Mille LS et al (2021) A smartphone-enabled portable digital light processing 3D printer. Adv Mater 33(35):2102153. https://doi.org/10.1002/adma.202102153
33. Maharjan S, Bonilla D, Sindurakar P et al (2021) 3D human non-alcoholic hepatic steatosis and fibrosis models. Bio-Des Manuf 4:157–170. https://doi.org/10.1007/s42242-020-00121-4
34. Li W, Mille LS, Robledo JA et al (2020) Recent advances in formulating and processing biomaterial inks for vat polymerization-based 3D printing. Adv Healthc Mater 9(15):2000156. https://doi.org/10.1002/adhm.202000156
35. Miri AK, Nieto D, Iglesias L et al (2018) Microfluidics-enabled multimaterial maskless stereolithographic bioprinting. Adv Mater 30(27):1800242. https://doi.org/10.1002/adma.201800242
36. Grigoryan B, Paulsen SJ, Corbett DC et al (2019) Multivascular networks and functional intravascular topologies within biocompatible hydrogels. Science 364(6439):458–464. https://doi.org/10.1126/science.aav9750
37. Yu C, Schimelman J, Wang PR et al (2020) Photopolymerizable biomaterials and light-based 3D printing strategies for biomedical applications. Chem Rev 120(19):10695–10743. https://doi.org/10.1021/acs.chemrev.9b00810
38. Fabris L, Perugorria MJ, Mertens J et al (2019) The tumour microenvironment and immune milieu of cholangiocarcinoma. Liver Int 39(S1):63–78. https://doi.org/10.1111/liv.14098
39. Lu P, Weaver VM, Werb Z (2012) The extracellular matrix: a dynamic niche in cancer progression. J Cell Biol 196(4):395–406. https://doi.org/10.1083/jcb.201102147

40. Papalazarou V, Salmeron-Sanchez M, Machesky LM (2018) Tissue engineering the cancer microenvironment-challenges and opportunities. Biophys Rev 10:1695–1711. https://doi.org/10.1007/s12551-018-0466-8
41. Torrino S, Grasset EM, Audebert S et al (2021) Mechano-induced cell metabolism promotes microtubule glutamylation to force metastasis. Cell Metabol 33(7):1342-1357.e10. https://doi.org/10.1016/j.cmet.2021.05.009
42. Krebs A, Mitschke J, Lasierra Losada M et al (2017) The EMT-activator Zeb1 is a key factor for cell plasticity and promotes metastasis in pancreatic cancer. Nat Cell Biol 19:518–529. https://doi.org/10.1038/ncb3513
43. Bordeleau F, Mason BN, Lollis EM et al (2017) Matrix stiffening promotes a tumor vasculature phenotype. Proc Natl Acad Sci USA 114(3):492–497. https://doi.org/10.1073/pnas.1613855114
44. Ma X, Qu X, Zhu W et al (2016) Deterministically patterned biomimetic human iPSC-derived hepatic model via rapid 3D bioprinting. Proc Natl Acad Sci USA 113(8):2206–2211. https://doi.org/10.1073/pnas.1524510113
45. Xu F, Kang TY, Deng J et al (2016) Functional nanoparticles activate a decellularized liver scaffold for blood detoxification. Small 12(15):2067–2076. https://doi.org/10.1002/smll.201503320
46. Loessner D, Meinert C, Kaemmerer E et al (2016) Functionalization, preparation and use of cell-laden gelatin methacryloyl-based hydrogels as modular tissue culture platforms. Nat Protoc 11:727–746. https://doi.org/10.1038/nprot.2016.037
47. Mao SS, He JY, Zhao Y et al (2020) Bioprinting of patient-derived in vitro intrahepatic cholangiocarcinoma tumor model: establishment, evaluation and anti-cancer drug testing. Biofabrication 12(4):045014. https://doi.org/10.1088/1758-5090/aba0c3
48. Sarker MD, Naghieh S, Sharma NK et al (2018) 3D biofabrication of vascular networks for tissue regeneration: a report on recent advances. J Pharm Anal 8(5):277–296. https://doi.org/10.1016/j.jpha.2018.08.005
49. Monteiro MV, Zhang YS, Gaspar VM et al (2021) 3D-bioprinted cancer-on-a-chip: level-up organotypic in vitro models. Trends Biotechnol 40(4):432–447. https://doi.org/10.1016/j.tibtech.2021.08.007
50. Stock K, Estrada M, Vidic S et al (2016) Capturing tumor complexity in vitro: comparative analysis of 2D and 3D tumor models for drug discovery. Sci Rep 6:28951. https://doi.org/10.1038/srep28951
51. Boucherit N, Gorvel L, Olive D (2020) 3D tumor models and their use for the testing of immunotherapies. Front Immunol 11:603640. https://doi.org/10.3389/fimmu.2020.603640